Formation of $O(^3P)$ Atoms in the Photolysis of N_2O at 193 nm and $O(^3P) + N_2O$ Product Channel in the Reaction of $O(^1D) + N_2O$

Satoshi Nishida, Kenshi Takahashi, and Yutaka Matsumi*

Solar-Terrestrial Environmental Laboratory and Graduate School of Science, Nagoya University, Honohara 3-13, Toyokawa, Aichi, 442-8507, Japan

Nori Taniguchi and Sachiko Hayashida

Faculty of Science, Nara Women's University, Kitauoya-Nishimachi, Nara, 630-8506, Japan

Received: October 9, 2003; In Final Form: December 23, 2003

The $O(^3P)$ atom produced in the 193 nm photolysis of N_2O has been detected by a technique of vacuum-ultraviolet laser-induced fluorescence spectroscopy around 130 nm. The quantum yield value of the $O(^3P)$ atoms produced directly in the photolysis of N_2O at 193 nm at room temperature has been determined to be 0.005 ± 0.002. The $O(^3P)$ atom formation process in the reaction of $O(^1D) + N_2O$ is also studied, and the channel branching ratio of $O(^3P) + N_2O$ has been determined to be 0.04 ± 0.02 among the product channels, 2NO, $N_2 + O_2$, and $O(^3P) + N_2O$. Photodissociation processes of N_2O at 193 nm and reaction processes of $O(^1D) + N_2O$ system have been discussed on the basis of the experimental results. Because of importance of the $O(^1D) + N_2O$ reaction in the stratosphere, impact of the experimental result of $O(^3P)$ formation from the $O(^1D) + N_2O$ reaction on the stratospheric chemistry is also studied by one-dimensional atmospheric model calculations.

1. Introduction

The gas-phase reactions of N_2O have been extensively studied because of its importance in atmospheric chemistry and chemical physics. The primary source of active nitrogen to the stratosphere on a global basis is from N_2O, which is released at the earth's surface through biological processes and to a smaller extent through anthropogenic activities.[1] Most of the N_2O molecules transported to the stratosphere are photolyzed at ultraviolet (UV) wavelengths around 200 nm. Photoabsorption of N_2O becomes significant below 240 nm, and its cross section has a maximum around 182 nm (1.47×10^{-19} cm^2 molecule^{-1}).[2,3] In the wavelength region, there are four energetically feasible pathways:

$$N_2O + h\nu \rightarrow O(^3P) + N_2(X^1\Sigma_g^+) \quad (\lambda < 742 \text{ nm}) \qquad (1a)$$

$$\rightarrow O(^1D) + N_2(X^1\Sigma_g^+) \quad (\lambda < 341 \text{ nm}) \qquad (1b)$$

$$\rightarrow N(^4S) + NO(X^2\Pi) \quad (\lambda < 252 \text{ nm}) \qquad (1c)$$

$$\rightarrow O(^1S) + N_2(X^1\Sigma_g^+) \quad (\lambda < 212 \text{ nm}) \qquad (1d)$$

where the long wavelength limit indicated in parentheses is the thermochemical threshold for each pathway.[2]

On the photodissociation of N_2O around 200 nm, channel 1b is dominant and the other channels are very minor.[3−6] Felder et al.[6] investigated the dissociation processes of N_2O at 193 nm using a photofragment translational spectroscopy and reported negligibly small yields of channels 1a, 1c, and 1d. Nakayama et al.[7] have recently measured the quantum yield of channel 1c to be $(2.1 \pm 0.9) \times 10^{-3}$ at 193 nm. Matsumi and Chowdhury[8] observed direct formation of small amounts of $O(^3P)$ atoms in the photolysis of N_2O at 193 nm. Recently, Brouard et al.[9] directly detected the $O(^3P_j)$ atoms from 193 nm photolysis of N_2O with the $O(3p^3P \leftarrow {}^3P_j)$ (2 + 1) REMPI transition near 226 nm. They studied the velocity and angular momentum alignment distributions of the $O(^3P_j)$ fragments using a technique of velocity map imaging.

In the stratosphere, in addition to the photodissociation, a small fraction of N_2O reacts with $O(^1D)$ atoms to yield NO molecules:

$$O(^1D) + N_2O \rightarrow NO(X^2\Pi) + NO(X^2\Pi) \qquad (2a)$$

$$\rightarrow N_2(X^1\Sigma_g^+) + O_2 \qquad (2b)$$

$$\rightarrow O(^3P) + N_2O \qquad (2c)$$

NO molecule reacts with O_3 very efficiently, which affects the photochemical balance of stratospheric O_3. The branching ratio for channel 2a is a critical parameter to investigate the O_3 balance because channel 2a is a predominant source of stratospheric NO_x. The NASA/JPL panel recommends the rate constants of $k_{2a} = 6.7 \times 10^{-11}$ and $k_{2b} = 4.9 \times 10^{-11}$ cm^3 molecule^{-1} s^{-1} at 298 K for use in stratospheric modeling studies.[3] The IUPAC subcommittee[4] evaluated the gas kinetic data for use in the studies of atmospheric chemistry and recommends the rate constants of $k_{2a} = 7.2 \times 10^{-11}$, $k_{2b} = 4.4 \times 10^{-11}$, and $k_{2c} < 1.0 \times 10^{-12}$ cm^3 molecule^{-1} s^{-1} at 298 K. Wine and Ravishankara[5] determined that the channel branching of $O(^3P) + N_2O$ (channel 2c) is <0.04, in which the $O(^3P)$ atom produced from the $O(^1D) + N_2O$ reaction was detected by the resonance fluorescence technique with a microwave-powered oxygen atomic lamp.

* Corresponding author: Fax +81-533-89-5593; e-mail matsumi@stelab.nagoya-u.ac.jp.

10.1021/jp037034o CCC: $27.50
Published on Web 03/09/2004

In this paper, we report the formation of $O(^3P)$ from N_2O photolysis at 193 nm (channel 1a) through the direct detection of the $O(^3P)$ atoms using a laser-induced fluorescence (LIF) technique. The quantum yield for channel 1a is determined experimentally. Moreover, we have studied the reaction of $O(^1D) + N_2O$ to produce $O(^3P) + N_2O$ (channel 2c) by the LIF technique and determined the channel branching ratio for channel 2c. Because of the atmospheric importance of the $O(^1D) + N_2O$ reaction, we also study the impact of the existence of channel 2c on the stratospheric chemistry by atmospheric model calculations with a one-dimensional dynamical and photochemical model. Changes in the steady-state concentrations of NO_x, O_3, and HO_x between the calculations with and without the new channel have been investigated.

2. Experiment

The experimental setup for the vacuum-ultraviolet laser-induced fluorescence (VUV-LIF) spectroscopic system used in this study has been described in detail elsewhere,[7,8,10−14] and we give only brief description pertinent to the current study here. The N_2O molecules were photolyzed by an ArF excimer laser at 193 nm (Lambda Physik, Compex 102). The typical photolysis laser pulse energies were 5 mJ at a repetition rate of 10 Hz. The $O(^3P_j)$ photofragments from N_2O photolysis were directly detected by the VUV-LIF technique using the $3s\ ^3S^0-2p\ ^3P_j$ transition at 130.22 nm for $j = 2$, 130.48 nm for $j = 1$, and 130.60 nm for $j = 0$. The VUV laser around 130 nm was generated by four-wave difference frequency mixing ($2\omega_1 - \omega_2$) in krypton gas,[15] using two dye lasers (Lambda Physik, FL3002 and Scanmate 2E) simultaneously pumped by a XeCl excimer laser (Lambda Physik, Compex 201). A typical pressure of Kr gas in the mixing cell was 15 Torr. The dye laser output was frequency-doubled in a BBO crystal to generate 212.56 nm for the ω_1 laser light, which was two-photon resonant with Kr $5p[1/2]_0$. The ω_2 laser light was tuned around 578.1, 572.8, and 570.6 nm for $O(^3P_j)$, $j = 2$, 1, and 0, respectively. The UV and visible laser beams were overlapped using a dichroic mirror and focused with a lens ($f = 200$ mm) into the Kr-containing cell. The generated VUV laser light was introduced into the reaction chamber through a LiF window. The bandwidth of the 130 nm VUV radiation was estimated to be 0.54 cm^{-1} (fwhm), which was determined by measuring the line width of thermalized $O(^3P_j)$ atoms.[12] A fraction of the incident VUV light passed through the photolysis chamber was reflected by a thin LiF plate held in the end of the photolysis chamber and led into a nitric oxide (NO) photoionization cell. The relative intensity of VUV laser light was monitored by measuring the photoionization current. Typical NO gas pressure was 2−3 Torr.

Huang and Gordon[16] reported the two-photon laser-induced fluorescence for $O(^3P)$ detection from the photodissociation of O_2 at 157 nm. The focused probe laser light at 226 nm excites the ground $O(^3P)$ atoms onto the $O(3p\ ^3P)$ state and the upper state fluoresces at 845 nm, thereby populating the $O(3s\ ^3S)$ state, which in turn fluoresces at 130 nm. They noticed that the probe laser produces a population inversion between the 3p and 3s levels, and ASE competes with normal fluorescence from the 3p state. The detection scheme we used in the present study is different from that of Huang and Gordon.[16] In our measurements, one-photon excitation scheme has been used to detect $O(^3P)$ atoms and the 3s state fluoresces only at 130 nm. ASE from the 3s state is impossible because the scheme we used is a two-level system. Furthermore, the VUV laser intensity is very weak ($<\mu$J/pulse) and not focused in the excitation zone. Thus, our measurements are applicable to the quantitative study of the photolytic and reactive $O(^3P)$ productions.

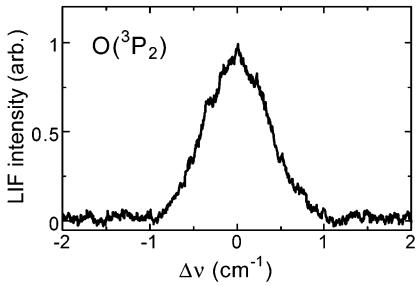

Figure 1. Vacuum-ultraviolet (VUV) laser-induced fluorescence (LIF) spectrum of $O(^3P_2)$ atoms produced in the 193 nm photolysis of N_2O, in which the VUV probe laser wavelength was scanned over the resonance line $O(3s\ ^3S^0-2p\ ^3P_2)$ at 130.22 nm. Partial pressures of N_2O and He in the reaction chamber were 22 mTorr and 1.7 Torr, respectively. The delay time between the photolysis and probe laser pulses was 200 ns.

The photolysis and probe laser beams was crossed at right angles. The time delay between the photolysis and probe laser pulses was controlled by a digital delay generator (Stanford Research Systems, DG535). The $O(^3P)$ VUV-LIF signal was detected at right angles to both photolysis and probe laser beams, using a solar-blind photomultiplier tube (EMR, 542J-09-17). The output from the photomultiplier was processed with a gated integrator (Stanford Research, SR-250) and stored on a personal computer.

The sample gases of N_2O (>99.9% purity), He (>99.99%), and N_2 (>99.99%) were used without further purification. Those gases were flowed into the reaction chamber through mass-flow controllers (STEC SEC-400s). The total pressure of the reactants in the chamber was measured with a capacitance manometer (Baratron, 122A).

3. Results

Figure 1 shows the typical fluorescence excitation spectrum of the $O(^3P_2)$ atoms produced from N_2O photolysis at 193 nm, in which the VUV probe laser wavelength was scanned over the resonance line $O(3s\ ^3S^0-2p\ ^3P_2)$ at 130.22 nm. The delay time between the photolysis and probe laser pulses was 200 ns. The pressures of N_2O and He were 22 mTorr and 1.7 Torr, respectively. The spectral width of the resonance line in Figure 1 is larger than that of thermalized $O(^3P_2)$ atoms. Brouard et al.[9] examined the velocity distributions of the $O(^3P_j)$ fragments by the velocity-map imaging technique and found that around 60% of the available energy appeared in product translation. Under our experimental conditions, the velocity distributions of $O(^3P_j)$ should be partly relaxed toward the Maxwell−Boltzmann distributions at room temperature due to the collisions with He buffer gas.[10] Figure 2 shows the fluorescence excitation spectra of $O(^3P_j)$, $j = 2$, 1, and 0, fine structure levels produced by the photodissociation of N_2O at 193 nm.

A linear dependence of the $O(^3P)$ LIF intensity on the photolysis laser power was checked, as shown in Figure 3. The $O(^3P)$ atoms produced by the photodissociation of N_2O were detected with the VUV-LIF method at the delay time of 200 ns between the photolysis and probe laser pulses under the pressure conditions of N_2O 22 mTorr and He 1.7 Torr. At the delay time of 200 ns, the detected $O(^3P)$ atoms are predominantly produced by the photodissociation of N_2O at 193 nm. No LIF signal of $O(^3P)$ without 193 nm laser light irradiation was observed. These results indicate that the multiphoton dissociation of parent N_2O at 193 nm and the photolysis of N_2O at 130 nm by the probe laser pulse can be ignored safely under our experimental conditions.

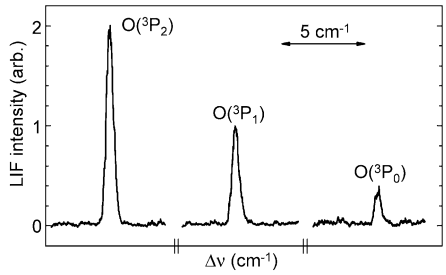

Figure 2. Fluorescence excitation spectra of O(^{3}P$_j$) atoms produced by the photolysis of N_2O. The center wavelengths for the $j = 2$, 1, and 0 spectra are 130.22, 130.48, and 130.60 nm, respectively. Partial pressures of N_2O and N_2 in the chamber were 50 mTorr and 1 Torr, respectively, and time delay was 10 μs.

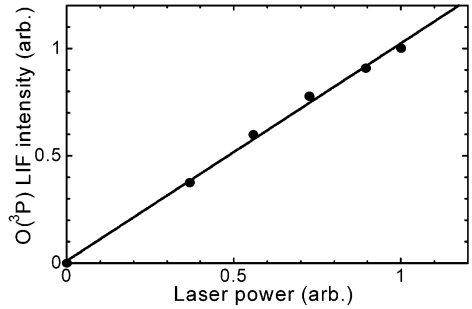

Figure 3. Plots of the O(^{3}P$_2$) LIF intensity vs the ArF photolysis laser power. N_2O molecules were photolyzed at 193 nm, and the resultant O(^{3}P$_2$) fragments were detected by the VUV-LIF method at 130.22 nm. The delay time between the photolysis and probe laser pulses was 200 ns.

We experimentally determine the values of the quantum yield for O(^{3}P) produced directly in the photolysis of N_2O at 193 nm (channel 1a) and the product channel branching ratio for O(^{3}P) + N_2O in the reaction of O(^{1}D) + N_2O (channel 2c). We detected the O(^{3}P) atoms using the VUV-LIF technique at the various delay times after the gas mixture of N_2O (22 mTorr) and buffer He gas (1.7 Torr) was irradiated with 193 nm laser pulses. The quantum yield of O(^{3}P) produced directly in the photolysis of N_2O is small, while the predominant product of the photolysis of N_2O is O(^{1}D) + N_2.[3,4,6] The collisional deactivation process of O(^{1}D) to O(^{3}P) by collisions with the He buffer gas atoms is very slow with the rate constant of $<7.0 \times 10^{-16}$ cm^3 molecule^{-1} s^{-1}.[17] The rate constant of O(^{1}D) with N_2O is 1.16×10^{-10} cm^3 molecule^{-1} s^{-1},[3] which is 10^5 times larger than the deactivation rate constant of O(^{1}D) by He. Therefore, the deactivation of O(^{1}D) by collisions with He was negligible, and the O(^{1}D) atoms produced in the photolysis of N_2O were removed by the reaction with N_2O under our experimental conditions of N_2O (22 mTorr) and He (1.7 Torr).

Figure 4 indicates the relative concentrations of the O(^{3}P) atoms as a function of the delay time, *t*, between the photolysis and probe laser pulses, when the gas mixture of N_2O (22 mTorr) and He (1.7 Torr) was photolyzed by the 193 nm laser pulse. The nonzero value of the O(^{3}P) atom concentration at the zero delay time is attributed to the direct formation of O(^{3}P) atoms by the photolysis of N_2O at 193 nm (channel 1a). Then, the O(^{1}D) atoms, which are the main atomic oxygen products in the photodissociation of N_2O at 193 nm (channel 1b),[3,4,6] react with N_2O molecules, and the additional O(^{3}P) atoms are produced through reaction process 2c. The gradual increase of the O(^{3}P) concentration with the increase of the delay time in Figure 4 corresponds to the reactive formation of O(^{3}P) through channel 2c.

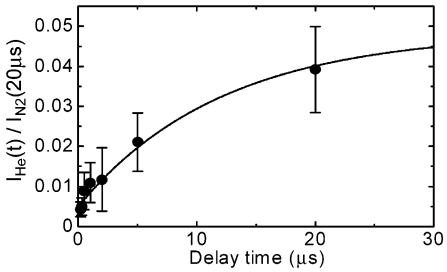

Figure 4. Relative concentrations of the O(^{3}P) atoms as a function of delay time between the photolysis and probe laser pulses, when the gas mixture of N_2O (22 mTorr) and He (1.7 Torr) was photolyzed by the 193 nm laser pulse. The vertical scale is the ratio of $I_{He}(t)/I_{N_2}(20\ \mu s)$, where $I_{He}(t)$ is the LIF intensity of O(^{3}P) with the gas mixture of N_2O/He at the delay time, *t*, and $I_{N_2}(20\ \mu s)$ is the LIF intensity of O(^{3}P) at the delay time of 20 μs with the gas mixture of N_2O (22 mTorr) and N_2 (0.7 Torr) instead of the N_2O/He gas mixture. The average values of $I_{He}(t)/I_{N_2}(20\ \mu s)$ and their standard deviation (1σ) for 5−10 times measurements at each delay time are plotted. The smooth curve indicates the best-fit curve with eq 4 in the text.

The O(^{3}P) atoms generated by the photolysis and reaction processes should have some excess translational energy. The translationally hot O(^{3}P) atoms are relaxed by collisions with the buffer gas molecules. Therefore, the spectral line shape of the O(^{3}P) atoms can change with the delay time. The nascent fine structure *j*-population of the O(^{3}P$_j$) produced by the photodissociation of N_2O at 193 nm is close to the degeneracy ratios of 0.56:0.33:0.11 for $j = 2$, 1, and 0, respectively.[9] The *j*-population of the O(^{3}P$_j$) is also relaxed by collisions to the Boltzmann distribution of 0.74:0.21:0.05 for $j = 2$, 1, and 0, respectively.[10] The *j*-population of the O(^{3}P) atoms produced from the deactivation reaction of O(^{1}D) through channel 2c is also relaxed by collisions.[11] Therefore, we measured the excitation spectra of O(^{3}P$_j$) at every delay time by scanning the probe VUV laser wavelength and then calculated the relative O(^{3}P) concentration by integrating the spectral peak areas.

Since the LIF signals of O(^{3}P) do not provide the absolute concentrations but the relative ones, a reference of the LIF intensity is required for the quantitative analysis to determine the quantum yield for channel 1a and the branching for channel 2c. The LIF intensity at the delay time of 20 μs after the photolysis of the gas mixture of N_2O (22 mTorr) and N_2 (0.7 Torr) instead of the N_2O/He gas mixture was used as the reference signal intensity, which is written as $I_{N_2}(20\ \mu s)$ hereafter. The vertical scale of Figure 4 is the ratio of $I_{He}(t)/I_{N_2}(20\ \mu s)$, where $I_{He}(t)$ is the LIF intensity with the gas mixture of N_2O (22 mTorr) and He (1.7 Torr) at the delay time, *t*, between the photolysis and probe laser pulses. The experimental procedure was as follows: first, the O(^{3}P$_j$) LIF intensity of $I_{He}(t)$ was measured with the N_2O/He gas mixture, and then that of $I_{N_2}(20\ \mu s)$ was measured with the N_2O/N_2 gas mixture. The partial pressure of N_2O gas was identical to be 22 mTorr between the N_2O/He and N_2O/N_2 mixture experiments. This procedure of alternative photolysis experiments was repeated 5−10 times at each delay time *t*. The average values of $I_{He}(t)/I_{N_2}(20\ \mu s)$ at each delay time, and their standard deviations (1σ) are plotted in Figure 4.

When the N_2O/N_2 gas mixture which was used to obtain the reference LIF intensity of $I_{N_2}(20\ \mu s)$ was irradiated with the 193 nm laser pulse, the O(^{1}D) atoms are first produced by the photodissociation of N_2O through channel 1b with the quantum yield of almost unity.[3,4,6] Then, the most of the O(^{1}D) atoms are deactivated to O(^{3}P) atoms by collisions with N_2 molecules:

$$O(^1D) + N_2 \rightarrow O(^3P) + N_2 \quad (3)$$

The quantum yield of the deactivation of $O(^1D)$ to $O(^3P)$ in the reaction of $O(^1D) + N_2$ is considered to be unity,[3,4] and the rate constant has been reported to be $k_3 = (2.6-3.1) \times 10^{-10}$ cm^3 molecule^{-1} s^{-1}.[3,18] Parts of the photolytically produced $O(^1D)$ atoms in the N_2O/N_2 gas mixture react with N_2O to yield the channel 2a−2c products. Under the pressure conditions of N_2O (22 mTorr) and N_2 (0.7 Torr), the calculation of $k_3[N_2]/k_2[N_2O]$ indicates that 87% of the $O(^1D)$ atoms produced from channel 1b are removed by reaction 3, while the residual 13% of them are removed by reaction 2. Since the lifetime of the $O(^1D)$ atoms in the N_2O/N_2 gas mixture is calculated to be $1/(k_3[N_2] + k_2[N_2O]) = 1.5$ μs, all of the $O(^1D)$ atoms have already removed and the concentration of the $O(^3P)$ atoms from channels 1a and 2c reaches an asymptote at the delay time of 20 μs. We checked that the concentration of $O(^3P)$ was almost constant at the delay time range of 10−30 μs. The diffusion loss of the $O(^3P)$ atoms was negligibly small in this delay time range. Moreover, the reaction of $O(^3P) + N_2O$ is inefficient at room temperature, so that it cannot affect the quantitative measurements of $O(^3P)$ in our experiments.[19,20]

The $O(^3P)$ LIF signal intensity ratios of $I_{He}(t)/I_{N_2}(20\ \mu s)$, which are plotted in Figure 4, are expressed as a function of the delay time t by

$$\frac{I_{He}(t)}{I_{N_2}(20\ \mu s)} = \frac{k_2[N_2O] + k_3[N_2]}{k_3[N_2]}[\Phi_{1a} + R_{2c}\{1 - \exp(-k_2[N_2O]t)\}] \quad (4)$$

where Φ_{1a} and R_{2c} ($\equiv k_{2c}/k_2$) are the quantum yield of $O(^3P)$ produced directly in the photolysis of N_2O at 193 nm (channel 1a) and the channel branching ratio of $O(^3P) + N_2O$ in the reaction of $O(^1D) + N_2O$ (channel 1b), respectively. $[N_2]$ corresponds to the partial pressure of N_2 (0.7 Torr) in the N_2O/N_2 gas mixture, while $[N_2O]$ is that of N_2O (22 mTorr), which is identical between the N_2O/He and N_2O/N_2 gas mixtures. Figure 4 shows that Φ_{1a} is not zero but quite small. This indicates $\Phi_{1b} \approx 1$. The approximation of $k_{2c}[N_2O] + k_3[N_2] \approx k_3[N_2]$ was used. The values of Φ_{1a} and R_{2c} have been determined by applying expression 4 to the plots in Figure 4 using a least-squares method. The values of $\Phi_{1a} = 0.005 \pm 0.002$ and $R_{2c} = 0.04 \pm 0.02$ were thus obtained. The uncertainties indicated for the Φ_{1a} and R_{2c} values include both the statistical errors (1σ) originating from a scattering of experimental data in the $I_{He}(t)/I_{N_2}(20\ \mu s)$ measurements and the systematic errors in the measurements of partial and total pressures.

4. Discussion

4.1. $O(^3P)$ Formation from N_2O Photolysis at 193 nm. In this study, the quantum yield for $O(^3P)$ formation in the 193 nm photolysis of N_2O has been determined to be 0.005 ± 0.002. The very small quantum yield value for $O(^3P)$ formation in the photolysis of N_2O at 193 nm is consistent with the previous studies reporting that the $O(^1D)$ atom formation (channel 1b) is dominant.[3,4,6] The lowest electronically exited singlet states of N_2O are the $A^1\Sigma^-$, the $B^1\Delta$, and the $C^1\Pi$ states. Upon bending the C_s symmetry group applies giving rise to the $1^1A'(^1\Sigma^+)$ and the $1^1A''(^1\Sigma^-)$ states. The Π and Δ states split into A′ and A″ components. Theoretical calculations of the electronic states of N_2O have been performed in relation to UV photodisociation[21,22] and $O(^1D) + N_2$ reaction process.[23] Figure 5 shows the correlation diagram for the reactions of $O + N_2$ and $NO + N$, in which C_s symmetry is assumed for the reaction intermediate.[20] The theoretical calculations by Hopper[21] have shown that dissociation around 200 nm occurs via the $2^1A'$ state and that the nearby $1^1A''$ state can also be involved in the dissociation process. Previous many studies showed that channel 1b is dominant with almost unity quantum yield in the 193 nm photolysis of N_2O,[3,4,6] which is rationalized by the fact that both the $2^1A'$ and $1^1A''$ states adiabatically correlate to the photoproducts of $O(^1D) + N_2(^1\Sigma^+_g)$.

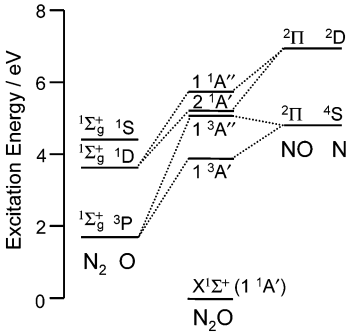

Figure 5. Adiabatic correlation diagram for N_2O system (N−NO, N_2O, and N_2−O) assuming a C_s symmetry in the intermediate, which is taken from the paper published by Hopper.[20]

The $O(^3P) + N_2(^1\Sigma^+_g)$ product state correlates to triplet states of N_2O. The adiabatic correlation diagram shown in Figure 5 suggests that the intersystem crossing from the exited singlet state to the triplet state or direct photoexcitation to the triplet state can account for the $O(^3P)$ formation. Nakamura and Kato[23] have calculated ab initio potential surfaces of three triplet states, $^3A''(^3\Sigma^-)$, $^3A'$, and $^3A''(^3\Pi)$, correlating with the asymptote $O(^3P) + N_2$, and studied the predissociation processes from the ground singlet state potential correlating with the $O(^1D) + N_2$ to the triplet states. Brouard et al.[9] have indicated that the dissociation to $O(^3P) + N_2$ takes place on the asymptotic $^3A''(^3\Sigma^-)$ surface, based on the measurements of the $O(^3P_j)$ velocity and angular momentum alignment parameters in the photolysis of N_2O at 193 nm. They have suggested that the photodissociation pathway to $O(^3P) + N_2$ involves either excitation to the $^1A'(^1\Delta_g)$ state, followed by transfer via a conical intersection to the $^1A'(^1\Pi)$ state, and a further crossing to the asymptotic $^3A''(^3\Sigma^-)$ surface, or direct triplet excitation to the $^3A''(^3\Sigma^-)$ state followed by the dissociation. A weak spin−orbit interaction between the singlet and triplet excited states or a small transition probability from the ground to the triplet states may results in the very small quantum yield for $O(^3P)$ formation in the N_2O photolysis at 193 nm. Adams et al.[24] probed the $N(^4S)$ atom formation (channel 1c) from N_2O photolysis at 207 nm using a two-photon LIF technique. Very recently, Nakayama et al.[7] measured the quantum yield for $N(^4S)$ formation through channel 1c using the VUV-LIF technique at 120.071 nm. The $N(^4S)$ quantum yield they reported is $(2.0 \pm 0.8) \times 10^{-3}$ in the N_2O photolysis at 193 nm. The $N(^4S) + NO(^2\Pi)$ product state also correlates to the triplet state(s) of N_2O. The nonnegligible contribution of the photoexcitation to the triplet state or the spin−orbit interaction between the singlet and triplet excited states to form $O(^3P)$ products is consistent with the reports on the detection of $N(^4S)$ products in the 193 nm photolysis of N_2O.

4.2. $O(^3P)$ Formation from $O(^1D) + N_2O$ Reaction. In this study, the product branching ratio of $O(^3P) + N_2O$ (channel 2c) in the reaction of $O(^1D) + N_2O$ has been determined to be 0.04 ± 0.02. Wine and Ravishankara[5] measured the branching

ratio for channel 2c to be <0.04 by means of time-resolved resonance fluorescence spectroscopic detection of $O(^3P)$ using an atomic oxygen lamp. In their study, they photolyzed the gas mixture of O_3/He/N_2O with a KrF excimer laser. The photolysis of O_3 at 248 nm produces both $O(^3P)$ and $O(^1D)$ atoms with the quantum yields of 0.09 and 0.91, respectively.[25,26] Thus, only the upper limit value for channel 2c was determined by them because the signal due to channel 2c in the time profile of $O(^3P)$ is very small compared with the direct formation of $O(^3P)$ from the O_3 photolysis under their experimental conditions. In our present study, we alternatively measured the $O(^3P)$ LIF intensities of $I_{He}(t)$ and $I_{N_2}(20\ \mu s)$ from the 193 nm photolysis of N_2O/He and N_2O/N_2 mixtures to determine the channel 2c branching ratio (R_{2c}). The high sensitivity of the VUV-LIF method for detection of $O(^3P)$ made it possible to use the N_2O photolysis at 193 nm as a source of $O(^1D)$ for the investigation of channel 2c in the reaction of $O(^1D) + N_2O$. Since the quantum yield for $O(^3P)$ formation from N_2O photolysis at 193 nm was found to be very small (0.005 ± 0.002), the production of $O(^3P)$ from channel 2c was clearly detected and analyzed quantitatively. An approximate rate constant of 4×10^{-12} cm^3 molecule^{-1} s^{-1} can be estimated for reaction 2c using our quantum yield (0.04 ± 0.02) and the recommended value for k_2 ($= 1.16 \times 10^{-10}$ cm^3 molecule^{-1} s^{-1}).

Since the electronic state of $O(^1D)$ is 5-fold degenerate, there are five potential energy surfaces (PESs) which asymptotically correlate to the $O(^1D) + N_2O$ reactants (two $^1A''$ and three $^1A'$ surfaces in C_s symmetry of N_2O_2 intermediate). On the other hand, there are three PESs which asymptotically correlate to the $O(^3P) + N_2O$ products (two $^3A''$ and one $^3A'$). From a theoretical point of view, the ab initio calculations of the N_2O_2 system have been performed.[27,28] Those theoretical studies focused on the reaction dynamics to generate channel 2a and 2b products. Although a possible interaction between the lowest $1^1A'$ and $^3A'$ PESs was suggested by the calculations of Last et al.,[27] the reaction process to generate channel 2c products was not discussed in their work. Further theoretical and experimental studies are required to elucidate the reaction process yielding the $O(^3P) + N_2O$ product and to understand the $O(^1D) + N_2O$ reaction system.

4.3. Atmospheric Implications. The $O(^1D) + N_2O$ reaction is a main source of the stratospheric NO_x. The NO_x molecules affect strongly the photochemical O_3 balance in the stratosphere.[1] Therefore, the channel branching for the formation of 2NO (channel 2a) over $N_2 + O_2$ (channel 2b) and $O(^3P) + N_2O$ (channel 2c) in the reaction of $O(^1D) + N_2O$ is an important parameter in the estimation of the production rate of NO_x in the stratosphere and the stratospheric O_3 concentration. Cantrell et al.[29] reported a measurement of $R_{2a} = 0.57$ and that an analysis of all measurements from 1957 to 1994 leads them to recommend a value of $R_{2a} = 0.61 \pm 0.08$, where the uncertainty indicates their 95% confidence interval. The latest NASA/JPL panel in 2003 recommends the rate constants of $k_{2a} = 6.7 \times 10^{-11}$ and $k_{2b} = 4.9 \times 10^{-11}$ cm^3 molecule^{-1} s^{-1} at 298 K for use in stratospheric modeling studies.[3] The individual product formation rates for the $O(^1D) + N_2O$ reaction in the NASA/JPL recommendations[3] are based on four experimental studies on the branching ratio measurements performed by Davidson et al.,[30] Volltrauer et al.,[31] Marx et al.,[32] and Lam et al.[33] The three studies of them measured the k_{2a}/k_{2b} value by detecting the reaction products of NO for channel 2a and N_2 or O_2 for channel 2b using the methods such as gas chromatography, chemiluminescence detection, and mass spectrometry.[30−32] Their values of k_{2a}/k_{2b} have been used to yield the R_{2a} ($\equiv k_{2a}/k_2$) value recommended in the NASA/JPL panel[3] on the assumption that only channels 2a and 2b are available as the products in the $O(^1D) + N_2O$ reaction. In this study, the channel 2c branching ratio has been determined to be 0.04 ± 0.02. The total reaction rate constant of the $O(^1D) + N_2O$ has been well determined experimentally. Therefore, the value of the channel branching R_{2a} should be decreased by about 4% by taking channel 2c into account. Since the uncertainty of the experimental results for the channel branching R_{2a} is still larger than 4% as indicated by Cantrell et al.,[29] the 4% change in R_{2a} does not seem to be much critical in atmospheric modeling studies. Nevertheless, it is worth estimating how sensitively the concentrations of atmospherically important species such as NO_x, O_3, and HO_x are affected by the change of the channel branching R_{2a} due to the existence of channel 2c.

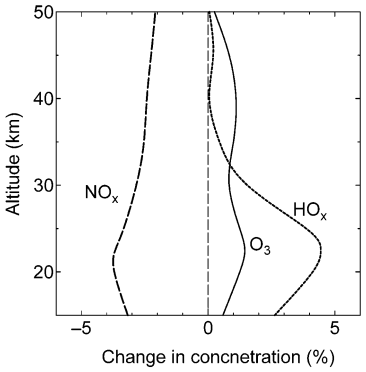

Figure 6. Percentage changes in diurnally averaged steady-state NO_x, HO_x, and O_3 concentrations calculated by a 1-D dynamical−photochemical model with or without channel of $O(^3P) + N_2O$ as products in the reaction of $O(^1D) + N_2O$. The model calculations have been performed for latitude of 40° in March as a function of altitude. The profiles of NO_x, HO_x, and O_3 are indicated by dash, dot, and solid curves, respectively.

We have investigated the impact of channel 2c on stratospheric chemistry by performing the one-dimensional photochemical and dynamical model simulations, in which the channel branching between (2a) and (2b) was reduced by 4% due to channel branching (2c). Details of the model have been described in our recent paper.[34] Briefly, all chemical schemes of the model are the same with those in the Garcia−Solomon two-dimensional (GS-2D) model.[35] The model calculations were performed including 40 chemical species and 120 chemical reactions with the chemical kinetics and photochemical data presented by the recent JPL recommendations.[3] Figure 6 shows the result of the photochemical model calculations for latitude of 40° in March, which indicates the changes in the diurnally averaged concentrations of NO_x, O_3, and HO_x ($= H + OH + HO_2$), calculated with or without channel 2c in the reaction of $O(^1D) + N_2O$. In the calculations, R_{2c} was assumed to be independent of temperature. The steady-state NO_x concentration calculated by the model including channel 2c decreases up to ~4% around 20 km in comparison with that ignoring channel 2c, while the HO_x and O_3 abundances increase. Perturbation in the concentrations of HO_x may be attributable to be associated with the following reaction:

$$OH + NO_2 + M \rightarrow HNO_3 + M \qquad (5)$$

As NO_x concentrations decreased due to the change in R_{2c} value, HO_x scavenged by reaction 5 increased. The concentration change of HO_x is larger in the lower stratosphere than those in the middle and upper stratosphere, as shown in Figure 6. This

is because that the contribution of three-body reactions (5) becomes more significant at higher air densities or at lower stratospheric altitudes. The chemical reactions involving NO_x and HO_x families play a crucial role in determining the stratospheric O_3 abundance,[1] and thus the concentration changes of these species alter O_3 abundance. Inclusion of channel 2c in the model affects the production rate of NO_x, which is followed by the increase of O_3 abundance through the reduction of the NO_x-catalyzed O_3 destruction rate.

5. Conclusions

The spin-forbidden formation process of $O(^3P) + N_2$ from the photodissociation of N_2O at 193 nm has been studied at room temperature. The high sensitivity of the vacuum-ultraviolet laser-induced fluorescence detection system allows us to analyze the direct formation of small amounts of $O(^3P)$ atoms quantitatively in the photolysis N_2O. The quantum yield of the $O(^3P) + N_2$ products (channel 1a) has been determined to be 0.005 ± 0.002. This value is as small as that of another spin-forbidden photodissociation process of $N(^4S) + NO(^2\Pi)$, which is $(2.0 \pm 0.8) \times 10^{-3}$.[7] These nonnegligible but small values of the quantum yields for the spin-forbidden photodissociation processes are attributed to a small transition probability of the direct photoexcitation to the triplet state or to weak spin−orbit interaction between the singlet and triplet excited states of N_2O. The formation of $O(^3P) + N_2O$ (channel 2c) from the reaction of $O(^1D) + N_2O$ has also been studied in this study. The product branching ratio for channel 2c has been determined to be 0.04 ± 0.02. The existence of channel 2c in the $O(^1D) + N_2O$ reaction affects the product branching for channel 2a that is important as a main source of NO_x in the stratosphere. We performed the one-dimensional photochemical and dynamical model simulations to estimate the impact of the new R_{2a} value on the stratospheric steady-state concentration of NO_x, HO_x, and O_3. We have suggested that the steady-state concentrations of NO_x, HO_x, and O_3 in the stratosphere are very sensitive to the change in the product branching ratios in the reaction of $O(^1D) + N_2O$ in consideration of channel 2c. The steady-state NO_x concentrations calculated by the model including channel of $O(^3P) + N_2O$ decrease up to ~4% around 20 km in comparison with that ignoring channel of $O(^3P) + N_2O$, while the HO_x and O_3 abundances increase.

Acknowledgment. This work was partly supported by Grants-in-Aid from the Ministry of Education, Science and Culture. The financial support by Sumitomo Foundation is also gratefully acknowledged. N.T. thanks the Japan Society for Promotion of Science for a fellowship for younger scientists.

References and Notes

(1) Brasseur, G. P.; Orlando, J. J.; Tyndall, G. S. *Atmospheric Chemistry and Global Change*; Oxford University Press: New York, 1999.

(2) Okabe, H. *Photochemistry of Small Molecules*; Wiley-Interscience: New York, 1978.

(3) Sander, S. P.; Friedl, R. R.; Golden, D. M.; Kurylo, M. J.; Huie, R. E.; Orkin, V. L.; Moortgat, G. K.; Ravishankara, A. R.; Kolb, C. E.; Molina, M. J.; Finlayson-Pitts, B. J. *Chemical Kinetics and Photochemical Data for the Use in Atmospheric Studies, Evaluation Number 14*; JPL Publication 02-25, JPL, Pasadena, CA, 2003.

(4) Atkinson, R.; Baulch, D. L.; Cox, R. A.; Hampson, Jr. R. F.; Kerr, J. A.; Rossi, M. J.; Troe, J. *J. Phys. Chem. Ref. Data* **1997**, *26*, 521.

(5) Wine, P. H.; Ravishankara, A. R. *Chem. Phys.* **1982**, *69*, 365.

(6) Felder, P.; Haas, B.-M.; Huber, J. R. *Chem. Phys. Lett.* **1991**, *186*, 177.

(7) Nakayama, T.; Takahashi, K.; Matsumi, Y.; Taniguchi, N.; Hayashida, S. *J. Geophys. Res.* **2003**, in press.

(8) Matsumi, Y.; Chowdhury, A. M. S. *J. Chem. Phys.* **1996**, *104*, 7036.

(9) Brouard, M.; Clark, A. P.; Vallance, C.; Vasyutinskii, O. S. *J. Chem. Phys.*, **2003**, *119*, 771.

(10) Abe, M.; Sato, Y.; Inagaki, Y.; Matsumi, Y.; Kawasaki, M. *J. Chem. Phys.*, **1994**, *101*, 5647.

(11) Matsumi, Y.; Inagaki, Y.; Morley, G. P.; Kawasaki, M. *J. Chem. Phys.* **1994**, *100*, 315.

(12) Takahashi, K.; Matsumi, Y.; Kawasaki, M. *J. Phys. Chem.* **1996**, *100*, 4084.

(13) Takahashi, K.; Taniguchi, N.; Matsumi, Y.; Kawasaki, M.; Ashfold, M. N. R. *J. Chem. Phys.* **1998**, *108*, 7161.

(14) Taniguchi, N.; Takahashi, K.; Matsumi, Y. *J. Phys. Chem. A* **2000**, *104*, 8936.

(15) Hilber, G.; Lago, A.; Wallenstein, R. *J. Opt. Soc. Am. B* **1987**, *4*, 1753.

(16) Huang, Y.-L.; Gordon, R. J. *J. Chem. Phys.* **1992**, *97*, 6363.

(17) Heidner III, R. F.; Husain, D. *Int. J. Chem. Kinet.* **1974**, *6*, 77.

(18) Ravishankara, A. R.; Dunlea, E. J.; Blitz, M. A.; Dillon, T. J.; Heard, D. E.; Pilling, M. J.; Strekowski, R. S.; Nicovich, J. M.; Wine, P. H. *Geophys. Res. Lett.* **2002**, *29*.

(19) Fontijn, A.; Goumri, A.; Fernandez, A.; Anderson, W. R.; Meagher, N. E. *J. Phys. Chem. A* **2000**, *104*, 6003.

(20) Meagher, N. E.; Anderson, W. R. *J. Phys. Chem. A* **2000**, *104*, 6013.

(21) Hopper, D. G. *J. Chem. Phys.* **1984**, *80*, 4290.

(22) Brown, A.; Jimeno, P.; Balint-Kurti, G. G. *J. Phys. Chem. A* **1999**, *103*, 11089.

(23) Nakamura, H.; Kato, S. *J. Chem. Phys.* **1999**, *110*, 9937.

(24) Adams, S. F.; DeJoseph Jr., C. A.; Carter, C. C.; Miller, T. A.; Williamson, J. M. *J. Phys. Chem. A* **2001**, *105*, 5977.

(25) Talukdar, R. K.; Longfellow, C. A.; Gilles, M. K.; Ravishankara, A. R. *Geophys. Res. Lett.* **1998**, *25*, 143.

(26) Takahashi, K.; Hayashi, S.; Matsumi, Y.; Taniguchi, N.; Hayashida, S. *J. Geophys. Res.* **2002**, *107*, 4440.

(27) Last, I.; Aguliar, A.; Sayós, R.; González, M.; Gilibert, M. *J. Phys. Chem. A* **1997**, *101*, 1206.

(28) Takayanagi, T.; Akagi, H. *Chem. Phys. Lett.* **2002**, *363*, 298.

(29) Cantrell, C. A.; Shetter, R. E.; Calvert, J. G. *J. Geophys. Res.* **1994**, *99*, 3739.

(30) Davidson, J. A.; Howard, C. J.; Schiff, H. I.; Fehsenfeld, F. C. *J. Chem. Phys.* **1979**, *70*, 1697.

(31) Volltrauer, H. N.; Felder, W.; Pirkle, R. J.; Fontjn, A. *J. Photochem.* **1979**, *11*, 173.

(32) Marx, W.; Bahe, F.; Schurath, U. *Ber. Bunsen-Ges. Phys. Chem.* **1979**, *83*, 225.

(33) Lam, L.; Hastie, D. R.; Ridley, B. A.; Schiff, H. I. *J. Photochem.* **1981**, *15*, 119.

(34) Taniguchi, N.; Hayashida, S.; Takahashi, K.; Matsumi, Y. *Atmos. Chem. Phys.* **2003**, *3*, 1293.

(35) Solomon, S.; Portmann, R. W.; Garcia, R. R.; Thomason, L. W.; Poole, L. R.; McCormick, M. P. *J. Geophys. Res.* **1996**, *101*, 6713.